Spin Relaxation from Continuous Film to Magnetic Nanostructures

X. Zhu[a,], Z. Liu[a], K. Buchanan[a], G. Woltersdorf[b], J. Liang[c], P. Grutter[d], V. Metlushko[e], A. Meldrum[a], J. Xu[c], B. Heinrich[b] and M. R Freeman[a]*
[a]Department of Physics, University of Alberta, Canada
[b]Department of Physics, Simon Fraser University, Canada
[c]Department of Electrical Engineering, Brown University
[d]Department of Physics, McGill University, Canada
[e]Dept of Electrical Engineering, University of Illinois at Chicago
**Contact author: xzhu@phys.ualberta.ca*

Abstract

The spin relaxation from continuous iron film, to lithographically patterned submicron Permalloy disks, and to iron and nickel nanoparticles were studied by ultrafast magnetooptical technique. In the continuous film, the damping parameter is obtained through fitting the experimental data. In the lithographically confined submicron disks, the excitation due to the formation of the standing waves is found. Ultrafast spin relaxation and spin relaxation due to magnetic coupling are investigated.

1. Introduction

Magnetization switching processes and spin dynamics in general are fundamental issues in magnetism, and are essential to technological applications such as magnetic storage and spintronics [1,2]. Time-domain measurements address the question of how fast a nonequilibrium magnetization relaxes, or what is the operating frequency limit of a magnetic device. In this article, we present a study of spin relaxation of ferromagnetic materials using ultrafast magnetooptical technique [3]. The purpose of this study is to investigate the evolution of spin relaxation as the ferromagnetic sample size shrinks. In the continuous film, ultrafast magntooptical technique is used to characterize the damping parameter of magnetization dynamics. In the laterally confined structures, the ultrafast magnetooptical technique is used to study the nonuniform magnetization dynamics. For magnetic nanostructures, the spin dynamics of the ensemble of nanoparticles are characterized.

2. Experimental Technique

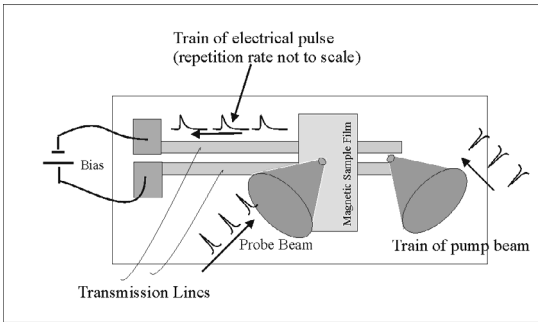

Figure 1. A representative setup of ultrafast magnetooptical experiments. The magnetic sample is placed on top of coplanar transmission lines, which are lithographically patterned on the semi-insulator GaAs semiconductor substrate. Focused pump beam will generate transient carriers in the focused region, which propagate through the bias transmission lines. The transient current gives rise to a transient magnetic field to perturb the magnetization of the sample out of the equilibrium. The resulting magnetization change is monitored through the focused probe beam. The time delay is controlled through changing the arrival time of the optical pulse using an optical delay line.

The schematic of the experimental setup is shown in Fig. 1. In this figure, a laser-triggered ultrafast magnetic field is used to perturb the sample's magnetization. A transient quasimetallic photoconductivity [4] induced by the pump pulse at the end of the coplanar transmission line structure launches a current pulse, which in turn drives the sample away from equilibrium with its associated transient applied magnetic field [5]. The change in the sample magnetization is measured magnetooptically,

Proceedings of the 2004 International Conference on MEMS, NANO and Smart Systems (ICMENS'04)
0-7695-2189-4/04 $20.00 © 2004 **IEEE**

and the signal averaged at a given time delay to achieve a sufficient signal-to-noise ratio. The time resolution is limited in principle only by the duration of the optical pulses, although in practice the resolution in the setup illustrated in Fig. 1 is limited to several picoseconds by dispersion of the electrical pulse as it propagates from the photoswitch to the specimen.

Note that if the probe beam is focused in between two transmission lines, the pulse field applied on the sample will be perpendicular to the substrate. However if the probe beam is focused onto a transmission line, the resulting pulse field will be mainly parallel to the sample substrate. The tradeoff of using photoconductive technique to produce an ultrafast field is that the peak field strength is usually small (less than 100 Oe). The magnetization is usually tipped away from its equilibrium at a very small angle. This technique is also called pulsed ferromagnetic resonance (FMR) or broadband FMR.

3. Experimental Results

The spin of magnetic materials in the classical limit can be described by the Landau-Lifshitz-Gibert (LLG) equation of motion [6]

$$\frac{\partial M}{\partial t} = \gamma[M \times H_{eff}] - \alpha\gamma[M \times M \times H_{eff}] \quad (1),$$

where γ is the gyromagnetic ratio, the absolute value of the electron spectroscopic splitting factor, M_s is the saturation magnetization and α is the dimensionless damping parameter. The effective field H_{eff} is produced by the exchange, magnetostatic crystalline anisotropy and Zeeman energies of the magnetization. The first term on the right hand side of the equation represents the precessional torque on the magnetization, which dictates the precession frequency, while the second term represents the damping torque, which is due to incoherent scattering of magnons, such as phonon and magnon scattering, relaxation via the spin-orbit interaction, or scattering due to magnetic inhomogenities.

3.1 Continuous Fe Ultrathin Film

Magnetic moments across ultrathin magnetic films are locked together by exchange coupling, which can be considered as giant magnetic moment. Magneitc Au/Fe(001) and Au/Cr/Fe(001) structures were prepared using molecular beam epitaxy (MBE) directly onto semi-insulating GaAs(001) wafers in ultrahigh vacuum [7]. The iron films are 16 atomic layers, while the Cr is 20 atomic layers. Both samples were covered by 20 atomic layers of Au for carrying experiments in ambient condition [8]. The magnetic anisotropy can be characterized as a four-fold volume anisotropy (same as bulk bcc iron) and a two fold anisotropy interface anisotropy due to surface bonding with GaAs substrate.

The time evolution of the magnetization of the out of plane component M_z was measured for different magnetic bias fields between 0 to 3 kOe. Fig. 2 shows two examples (Au/Fe/GaAs and Au/Cr/Fe/GaAs) of broadband FMR measurements. Clearly, the relaxation for Au/Cr/Fe/GaAs appears to be much faster compared to Au/Fe/GaAs. The sample's initial magnetization is aligned along its in-plane easy axis using a bias field of 1 kOe. A transient field generated by current from a photoconductive switch is applied perpendicular to the sample plane, which causes the magnetization to tip away from the equilibrium direction, initiating a subsequent precession about the bias field direction. The change of magnetization perpendicular to the plane is monitored by the probe beam using the polar Kerr effect. The damping of the magnetization resonance can be measured directly from the gradual decrease with time of the oscillation amplitude. Another interesting characteristic of this curve is that the resonant oscillation is superimposed on the shape of the magnetic field pulse, which has a fast rise time but relatively slower decay dictated by the approximately 250 ps carrier lifetime in the semi-insulating GaAs photoswitch. The overall behavior can be well described by the Equation 1. The parametric following of the pulse shape is due to the fact that at frequencies below resonance, the magnetization responds quasistatically to the change of the magnetic field. For larger bias fields, the precessional angle of the magnetization will decrease in addition to the frequency increasing, and eventually the measured magnetization change becomes a map of the real pulse shape.

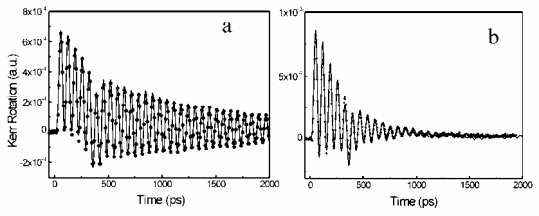

Figure 2. The change of the out of plane component of magnetization M_z versus ultrafast magnetic field pulses. (a) continuous film of 16 atomic layers of Fe on GaAs substrate covered by 20 atomic layers of Au at a bias field of 1 kOe applied along easy axis. (b) continuous film of 16 atomic layers of Fe covered with 20 atomic layers of Cr and 20 atomic layers of Au at a bias field of 1.1 kOe. Dots: experiment, lines: fit.

In the ultrathin film, the magnetization can be approximated as a single spin. The spin relaxation precession can therefore be fitted using Eq. 1 after considering the magnetic pulse shape and the effective field. The fitting results are the solid lines in Fig. 2. The damping parameter for Au/Fe/GaAs is α = 0.0037, while it is 0.02 for Au/Cr/GaAs. The step-induced spin frustration in antiferromagnetic Cr behaves like magnetic inhomogenity at the Fe/Cr interface, which gives rise to increased damping parameter. Detailed study indicates that the increase of the damping parameter is due to two-magnon scattering in the sample plane [7,8]. The Cr cover layer not only causes a two magnon scattering effect, but also increases the coercive field from 5 Oe from Au/Fe/GaAs to 30 Oe, and strongly changes the magnetic anisotropies.

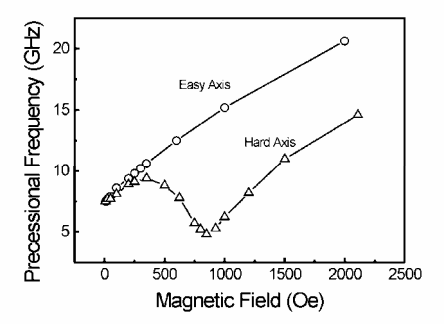

Figure 3. Frequency vs. bias field for the 20Au/16Fe/GaAs sample. Dots were obtained with the bias field applied along the easy axis [110]; triangles were obtained with the bias field applied 1.2° off the hard axis.

Besides characterizing the damping parameter through fitting FMR data. The precessional frequency as a function of the bias field along easy and hard directions can be used to determine the intrinsic parameter such as g-factor. Fig. 3 shows the precessional frequency changes at different external bias field changes. Note that due to magnetic anisotropies, the precessional frequency in response to external magnetic field is also anisotropic.

3.2 Submicron Permalloy Disks: Nonuniform Excitation

Permalloy disks with the size from 200 nm to 1 μm and the thickness from 25 to 50 nm were prepared by either optical lithography or electron beam lithography technique. The permalloy disks with the diameter of 700 nm and the thickness of 40 and 50 nm were prepared on 100 nm thick SiN_x membrane, while other sample were prepared on the silicon substrate.

For laterally confined structures, the demagnetized field inside the sample is generally non-uniform, as a result, the magnetic moment will not precess coherently. Instead, the magnetic moment will precess at different frequencies at different location governed by its local field [9,10]. For lithographically patterned magnetic structures, magnetically soft disk is very unique, as the magnetic vortex is usually energetically stable [11]. In the vortex state, the magnetization is circulating around the disk center with the central magnetization (vortex core) perpendicular to the disk plane [12,13]. The representative magnetic force microscopy images of these structures are shown in Fig. 4. The vortex state has also been demonstrated through Lorentz microscopy imaging.

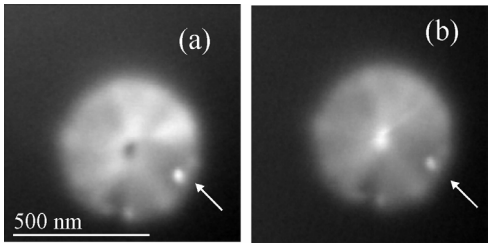

Figure 4. (a) and (b) two different vortex states of the same permalloy disk with a diameter of 500 nm and a thickness of 30 nm. The images show low contrasts due to the magnetic moment circulating around the center, resulting in low stray field above the disk. The dark or white center is a vortex core singularity with the magnetic moment pointing into or out of the disk plane. Arrows point to the same topography artifact, demonstrating that the central bright or black spot is magnetic.

Unpatterned sample shows uniaxial anisotropy with the coercivity of 2.5 Oe. The switching behavior of submicron permalloy disks is vortex nucleation, displacement and annihilation process [11,13]. High magnetic field with the order of a few hundred

oersteds is required to push the vortex core out of the disks. The precessional frequency for the vortex state is very different from continuous film. Fig. 5a shows the Kerr rotation as a function of time for unpatterned film at an external bias field of 6 Oe applied along the easy axis. The field pulse is applied perpendicular to the sample plane. The precessional frequency is very low (1 GHz). The relation between the precessional frequency and external bias field can be described by a Kittel relation. Different from unpatterned film, the precessional frequency of the permalloy disk in vortex state is very high. Fig. 5b shows the spin relaxation of 500 nm Permalloy disk with the pulse field applied perpendicular to the disk plane. The precessional frequency is found to be 10.5 GHz. The high frequency oscillation is due to the fact that the magnetic moment inside the disk is nonuniform, which gives rise to a higher effective precessional field. This can be explained analytically by solving the Lamor equation [14]. The precessional frequency can be described as following: $f_{th}=1/2\pi M_s\gamma M_s(N_\rho N_z)^{1/2}$, *where,* γ *is gyromagnetic ratio of* 1.76×10^7, $M_s=800$ *emu/cm*^{3}, N_ρ *and* N_z *is the demagnetized factor in the radial direction and perpendicular to the disk plane respectively [14,15]. The theoretical precessional frequency is found to be 10 GHz. The result is also consistent with micromagnetic modeling as shown in the solid line in Fig. 5b. The strong uniform excitation in the disk is due to the fact that the external pulse field is uniformly applied on the magnetization in the disks, and all magnetic moments in the disk experience same torque except the central vortex core area, where the magnetization is almost parallel to the pulse field resulting little precessional motion.*

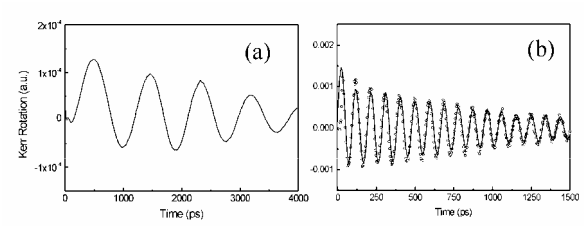

Figure 5. (a) Broadband FMR of $Ni_{80}Fe_{20}$ *film at a bias field of 6 Oe applied along the easy axis; (b) FMR curve of* $Ni_{80}Fe_{20}$ *disk with the disk diameter of 500 nm; The dots are experimental result, and the line is obtained by micromagnetic simulations.*

If the pulse field generated from transmission lines is applied in the disk plane, initial non-uniform precessional torque will be produced as a result of the nonuniform magnetization. The initial motion of the magnetic moments inside the disk will precess at different frequencies and different phases, resulting in nonuniform spin relaxation as shown in Fig. 6. Fig. 6a shows the out of plane component of magnetization of a 700 nm disk with the pulse field almost parallel to the disk plane. Fig. 6b is the Fourier transfer of the Fig. 6a, showing multiple precessional frequencies. Among these frequencies, there is a dominant one at around 0.4 GHz, which corresponds to the relaxation of the vortex core. The initial displacement of the vortex core in response to the in-plane pulse field gives rise to a nonzero torque (restoring force) toward the disk center, which produces the circular motion around the center [9,16]. Recently, the trajectory of the vortex core has also been observed in real space using time-resolved x-ray imaging [17], which demonstrates that the magnetization dynamics is determined by its handedness, and the initial acceleration of the vortex is parallel to a field pulse.

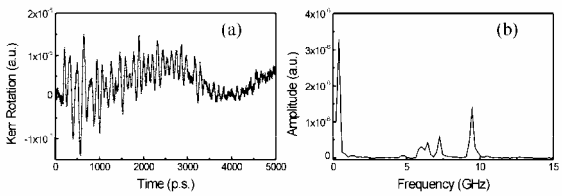

Fig. 6 (a) FMR curve of a 700 nm permalloy disk, with an in plane pulse field applied.; (b) FFT of (a), showing multiple precessional frequencies.

Higher frequency modes in Fig 6b correspond to the different standing wave patterns in the disks. At vortex state, the magnetization is circulating, so the spin wave pattern corresponding to azimuthal modes can be formed. Because of the existence of the vortex core (acting as apinning site), radial modes can also be formed. The experimental results can be explained through micromagnetic simulations. When a perpendicular transient pulse is applied, only 'uniform' mode is excited. However, if we plot the frequency spectrum at different location in the disk, we find that excitation modes corresponding to the standing wave pattern can be formed, but their frequency amplitude is much smaller compared to the 'uniform' excitation modes. In-plane pulse produces nonuniform torque in the disk, which acts like a nonuniform pulse field, and the multiple standing wave modes are excited.

3.3 Magnetic Nanostructures

The preparation of magnetic nanoparticles with a controlled particule size and spatial location is currently of significant technological interest for ultrahigh-density magnetic storage media [18,19] or information propagation [20]. There are many ways to produce magnetic nanoparticles, such as self-assembly [21], electron beam lithography [18], and nanoimprint [19,22]. In this session, we will present the study of spin dynamics of two different kinds of magnetic nanoparticles. One sample was prepared by ion implantation, the other sample is prepared by anodized aluminum oxide (AAO) membrane [23]

3.3.1. Nanoparticle made by ion implantation

Recent work has shown that ion implantation and thermal processing techniques can be used to form embedded nanoparticles [24]. Iron particles in SiO_2 were prepared by ion implantation followed by thermal annealing. Transmission electron microscopy (TEM) micrographs, as shown in Fig. 7a, indicate that sample contains spherical nanoclusters of iron with diameters of around 10 nm concentrated within the top 60 nm, however, particles as large as 20 nm in diameter were observed. Electron diffraction measurements reveal the presence of crystalline iron in the bcc (ferromagnetic) form. The filling factors were estimated from plan view micrographs of the specimens to fall in the 40 to 50 % range. Therefore, the nanoparticles will be strongly coupled.

Magnetooptical Kerr effect hysteresis loop indicates that the easy axis of magnetic particles lies in plane due to dipolar coupling. The coercivity is 46 Oe for the sample annealed at 600 ^{o}C. Fig. 7b shows the magnetization relaxation of the iron nanocomposite in the presence of in-plane bias fields ranging from 0 to 3 kOe. Overall, the temporal response follows the expected pulse shape with small oscillations superimposed. It is difficult to directly obtain the precessional frequency from Fig. 7b, especially for intermediate bias field, where few oscillation cycles are observed. However, the rise time of magnetization M_z is an alternative measure of the precessional frequency. The rise time is defined as the time for the Kerr signal increase from 10% to 90% of the maximal Kerr rotation for initial pulse field excitation. The rise time as a function of the bias field is shown in Fig. 7c. As the in-plane bias field increases, the rise time varies smoothly from small to large and then large again. The precessional frequency as a function of the bias field goes to the opposite way. As the bias field increases, the precessional frequency decreases to a minimum at the external bias field around 400 Oe then increases as the bias field increases. Note that from the hysteresis measurement, 400 Oe is also the field required to saturate the magnetization of the sample in plane.

The fast precessional mode or small rise time at small bias is due to the magnetostatic coupling. Micromagnetics simulations indicate that in-plane stripe-like patterns are formed at small bias field. The magnetic structures of the sample has also been imaged by magnetic force microscopy, and the domains with size of less than 100 nm have been revealed. Theoretical analysis indicates that the coupling produces a large effective to each individual nanoparticles, resulting in higher precessional frequency [25]. Fig. 6d shows the simulation at zero bias. Quite good agreement with the experimental data is obtained. For higher in-plane magnetic fields, the magnetization vectors of all of the individual clusters tend to align along the direction of the external bias field H_{bias} and the particles oscillate coherently.

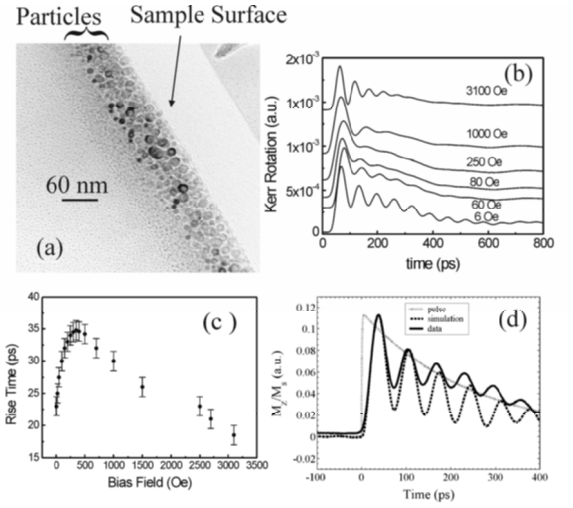

Figure 7 (a) cross section transmission electron microscopy images of as-implantated iron in SiO_2, (b) pulsed ferromagnetic resonance at different bias field from 6 Oe to 3100 Oe, (c) rise time as a function of external bias field, (d) ferromagnetic resonance data at remanence for experimental results (solid line) and simulation (dashed line). Dotted line in (d) is the pulse shape.

3.3.2. Nanoparticle made by AAO membrane

Recently, it has attracted great interest of preparing magnetic nanoparticles using anodized aluminum oxide (AAO) membrane as a mask [23]. This technique

provides better control of particle size compared to ion implantation. The nanoparticles studied in this section are Ni particles. The average diameter of nickel particles is about 50 nm with the nominal height of 30 nm. The particles form truncated conical shape with the height-diameter aspect ratio around 0.6. The variation of the particle diameter is due to atom diffusion during deposition and surface roughness. The pore size variation of AAO membrane has less contribution the particle size variation. The magnetization of the particles prefers to stay out of plane. This has been confirmed through magnetic force microscopy imaging, as shown in Fig. 8a. The black or white contrast from each individual nanoparticles indicates that the magnetization is attractive or repulsive to the MFM tip. Out of plane configuration for low aspect ratio particle has also been observed in other research groups [26,27], which is also consistent with theoretical calculation [28].

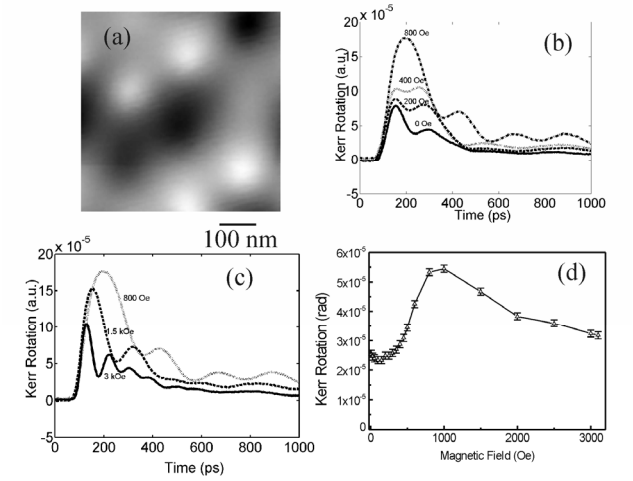

Figure 8. (a) Magnetic force microscopy image of Ni particle array; (b) Spin dynamics as a function of in-plane bias field from 0 Oe to 800 Oe; (c) Spin dynamics with the bias field from 800 Oe to 3 kOe; (d) the maximum Kerr rotation as a function of external bias field.

Figs 8b and 8c show the pulsed FMR at different in-plane bias field. The obtained results are very different from Fe particles prepared by ion implantation. The particles show little oscillations at remanence. Based on MFM images, the magnetic moments inside the dots are perpendicular to the substrate. However, as the particle size is still much bigger than the exchange length of Ni (a few nanometers), the magnetization inside the dot is not necessary uniformly magnetized. For example, 'flower' magnetic configuration could be formed [27]. In response to an ultrafast pulse field, the precessional motion of each 'unit' inside the particle isn't coherent due to different local field and different precessional phase. In addition, since the signal measured is an average of over 100 individual particles (assuming 1μm probe size beam size), the particle size variation and magnetic dipolar interaction can also broaden the FMR curve. Due to these effects, little oscillations have been observed at low bias field. In another word, these effects substantially increase the effective damping parameter for the spin relaxation of particle array.

At very high external bias field (> 800 Oe), shown in Fig. 8c, the magnetization inside the particles is mainly aligned in the substrate plane, and the external bias field is the dominant force for the precessional motion. The precessional motion is observed. As the bias field increases, the precessional frequency increases.

For uniform magnetized sample, maximal Kerr rotation in response to pulsed field usually decreases as the external bias field increases. For truncated conical nickel particles, shown in Fig. 8d, we find that the maximal Kerr rotation increases as the in-plane bias field increases when the bias field is smaller than 800 Oe, while it decreases as the bias field increases when the bias field is larger than 800 Oe, as shown in Fig. 8d. This nonmonotonic behavior is the result of magnetization transition from perpendicularly magnetized state to in-plane magnetized state. For small bias field, since the magnetic moment is mainly perpendicular to the disk plane, in response to a transient field perpendicular to the sample plane, the torque is very small, which gives rise to small Kerr rotation. As the in-plane bias field increases, the magnetization will rotate out of the disk plane, and the angle between the magnetization and pulse field increase, which increases the torque, giving rise to larger Kerr rotation. The effect of the external field will also stiffen the magnetization especially when the magnetization is aligned in plane. The Kerr rotation will decrease as the bias field increases, as expected.

4. Summary

The pulsed FMR has been used to study the continuous magnetic film, magnetic microstructures and magnetic nanostructures. In the continuous film, the magnetic moments can be considered as a single giant spin, and their precessional motion is coherent. Through fitting the FMR curve, the damping parameter can be obtained. The magnetic moment configuration inside

lithographically patterned structures is usually nonuniform, and precessional motion is spatially inhomogeneous. In some symmetrical structures such as a Permalloy disk, the standing wave patterns can be formed. The spin relaxation in magnetic nanostrucutre is a complex due to less understanding the magnetization configuration inside these small structures. For the magnetic nanostructures, the precessional motion strongly depends on magnetic structure itself and their coupling. These effects may limit the storage density, and their switching speed.

5. Acknowledgments

The work is supported by NSERC (Canada), iCORE, and CIAR. The author X. Z. is also thankful for the support from Alberta Ingenuity Fund.

6. References

[1] S. Parkin, X. Jiang, C. Kaiser, A. Panchula, K. Roche. M. Aamant, "Magnetically engineered spintronic sensors and memory", Proceedings of the IEEE, **91** *(2003) pp. 661-680.*

[2] S. A. Wolf, D. D. Awschalom, R. A. Buhrman, J. M. Daughton, S. von Molnar, M. L. Roukes, A. Y. Chtchelkanova, and D. M. Treger, "Spintronics: A spin-based electronics vision for the future", Science, **294** *(2001) pp. 1488-1495.*

[3] M. R. Freeman and W. K. Hiebert, "Stroboscopic microscopy of magnetic dynamics", in Spin Dynamics in Confined Magnetic Structures I, B. Hillebrands and K. Ounadjela, eds., Springer 2002.

[4] D. H. Auston, "Impluse-response of photoconductors in transmission-lines" IEEE J. Quantum Electron, **QE-19** *(1983) pp. 639-648.*

[5] M. R. Freeman, R. R. Ruf, R. J. Gambino, "Picosecond pulsed magnetic-fields for studies of ultrafast magnetic phenomena", IEEE Trans Mag., **27** *(1991) pp. 4840-4842.*

[6] L. D. Landau, E. M. Lifshitz, Mechanics and Electrodynamics, (Pergamon, Oxford, 1972).

[7] R. Urban, B. Heinrich, G. Woltersdorf, K. Ajdari, K. Myrtle, J. F. Cochran, and E. Rozenberg, "nanosecond magnetic relaxation processes in ultrathin metallic films prepared by MBE", Phys. Rev. B, **65** *(2001) pp. 020402-020405.*

[8] Georg Woltersdorf, Ph.D. Thesis, Simon Fraser University, 2004.

[9] J. P. Park, P. Eames, D. M. Engebretson, J. Berezovsky and P. A. Crowell, "Imaging of spin dynamics in closure domain and vortex structures", Phys. Rev. B, **67** *(2003) pp. R020403-020406.*

[10] M. Belov, Z. Liu, R. D. Sydora, and M. R. Freeman, "Modal oscillation control in internally patterned $Ni_{80}Fe_{20}$ thin film microstructures", Phys. Rev. B., **69** *(2004) pp. 094414-094418.*

[11] R.P. Cowburn, M. Wellend, "Single-domain circular nanomagnets", Phys. Rev. Lett,. **83** *(1999) pp. 1042-1045.*

[12] T. Shinjo, T. Okuno, R. Hassdorf, K. Shigeto, and T. Ono, "Magnetic vortex core observation in circular dots of permalloy", Science, **289** *(2000) pp. 930-932.*

[13 X. Zhu, P. Grutter, V. Metlushko, B. Ilic, "Magnetization reversal and configurational anisotropy of dense permalloy dot arrays", Appl. Phys. Lett,. **80** *(2002) pp. 4789-4791.*

[14] Y. Acremann, C. H. Back, M. Buess, O. Portmann, A. Vaterlaus, D. Pescia, and H. Y. Melchior, "Imaging precessional motion of the magnetization vector", Science, **414***, (2001) pp.51-54.*

[15] D. Chen, J. A. Brug, and R. B. Goldfarb, "Demagnetized factors for cylinders", IEEE Trans. Mag., **27** *(1991) pp. 3601-3619.*

[16] K. Yu Guslenko, B. A. Ivanov, V. Novosad, Y. Otani, H. Shima, K. Fukamichi, "Eigenfrequencies of vortex state excitations in magnetic submicron-size disks " J. Appl. Phy., **91** *(2002) pp. 8037-8039.*

[17] S-B. Choe, Y. Acremann, A. Scholl, A. Bauer, A. Doran, J. Stohr, and H. A. Padmore, "Vortex core-driven magnetization dynamics", Science, **304** *(2004) pp. 420-422.*

[*18*]*S. Y. Chou,* **"***Patterned magnetic nanostructures and quantized magnetic disks", Proceedings of the IEEE,, 85 (1997) pp. 652-671.*

[19] M. Albrecht, C. T. Rettner, A. Moser, M. E. Best, and B. D. Terris, "Recording performance of high-density patterned perpendicular magnetic media", Appl. Phys. Lett., **81** *(2002) pp. 2875-2877.*

[20] R. P. Cowburn and M. E. Welland, "Room Temperature Magnetic Quantum Cellular Automata", Science, **287** *(2000) pp. 1466-1468.*

[21] J. *Cheng, C. A. Ross, E. L. Thomas, H. I. Smith, and G. J. Vancso, "Templated self-assembly of block copolymers: Effect of substrate topography", Advn. Materials,* **15***, (2003) pp. 1599*

[22] S. Y. Chou, C. Keimel, J. Gu, "Ultrafast and direct imprint of nanostructures in silicon", Nature, **417** *(2002) pp. 835-837.*

[23] J. Liang, H. Chik, A. Yin and J. Xu, "Two-dimensional lateral superlattices of nanostructures: Nonlithographic formation by anodic membrane template", J. Appl. Phys., **91** *(2002) pp. 2544-2546.*

[24] Honda, F. A. Modine, A. Meldrum, J. D. Budai, T. E. Haynes, and L. A. Boatner, "Magneto-optical effects from nanophase -Fe and Fe_3O_4 precipitates formed in yttrium-stabilized ZrO_2 by ion implantation and annealing", Appl. Phys. Lett., **77** *(2000) pp. 711-713.*

[25] K. Buchanan, Ph.D. Thesis, University of Alberta, 2004.

[26] G. Meier, M. Kleiber, D. Grundler, D. Heitmann, and R. Wiesendanger, "Vertical polarization of quantum magnets in high density arrays of nickel dots with small height-to-diameter ratio", Appl. Phys. Lett. **72** *(1998) pp. 2168-2170.*

[27] C. A. Ross, M. Farhoud, M. Hwang, H. I. Smith, M. Redjdal, and F. B. Humphrey, "Micromagnetic behavior of conical ferromagnetic particles," J. App. Phys. **89,** *(2001) pp. 1310-1319.*

[28] J. Escrig, P. Landeros, J. C. Retamal, and D. Altbir, "Magnetic behavior of nanoparticles in patterned thin films", Appl. Phys. Lett. **82,** *(2003) pp. 3478-3480.*